

## Development of an Electrochemical Biosensor for Rapid Detection of Foodborne Pathogenic Bacteria

Yi Wu and Hui Chai\*

College of Life Science, Zhejiang Chinese Medical University, Hangzhou 310053, P.R. China

\*E-mail: [huichai\\_zcmu@126.com](mailto:huichai_zcmu@126.com)

Received: 29 January 2017 / Accepted: 6 March 2017 / Published: 12 April 2017

---

The development of quick, sensitive and targeted approaches to detect foodborne pathogenic bacteria is very critical to the implementation of efficient practice to guarantee food security. We reported the results of research relevant to fabrication of the graphene wrapped copper (II) assisted cysteine hierarchical structure (rGO-Cu(II)) synthesised under moderate, aqueous as well as eco-friendly conditions. A super sensitive unmarked electrochemical immunosensor for quantitative assay of *Staphylococcus aureus* has been formed with the use of rGO-Cu(II) as the sensing layer..

---

**Keywords:** Pathogenic bacteria; Graphene; Nanocomposite; *Staphylococcus aureus*; Immunosensor

### 1. INTRODUCTION

For decades, foodborne pathogens have posed a great risk to human health and food security and they are still being worried by the public. Nowadays, over 250 diseases known already are resulted from diverse foodborne pathogenic microorganisms, such as pathogenic viruses, parasites, viruses, bacteria and so on. Among them, the one with the highest occurrence frequency is bacteria, which takes up 91% of the appearance of foodborne diseases in America [1]. According to estimates, about 76 million illnesses were resulted from foodborne pathogens, in which there were 325.000 hospitalizations as well as over 5000 deaths in America every year [2]. In addition, the treatment of foodborne illnesses is very costly. It is estimated by the U.S. Department of Agriculture (USDA) Economic Research Service (ERS) that the medical charges as well as losses of production related to five main pathogens, namely *E. coli* O157:H7, *Salmonella* (non-typhoidal serotypes only), non-O157 STEC (Shiga Toxin-Producing *Escherichia coli*), *Listeria monocytogenes* and *Campylobacter*, is \$6.9 billion every year to say the least. The sustained explosion of diseases and the corresponding revocation of food products on account of foodborne pathogens set off the alarm bell for the Federal

Government, bringing much stress on regulatory as well as inspection organizations. Previously in the 1900s, the Federal Government started to form regulatory programs in the field of food safety, and later in 1998, it implemented the President's Council on Food Safety, revealing that it had made many efforts to ensure food security in America through various means. At present, the regulation of food safety as well as the development of novel inspection approaches is supervised mainly by three organizations, namely the Food Safety and Inspection Service (FSIS) within the USDA, the Environmental Protection Agency (EPA), and the Food and Drug Administration (FDA) within the Department of Health and Human Service (HHS). Moreover, the Institute of Food Technologists (IFT) has developed the method of Hazard Analysis Critical Control Point (HACCP) that can be regarded as one fundamental step in the current as well as future of food security countrywide and globally [3]. The problem of foodborne pathogens has caught the sight of several fields, including the science circles, food industry, academic world as well as the public which has become more and more recognized and worried about the health threats brought by foodborne pathogens.

Monitoring is the first point of reference in preventing illnesses resulted from foodborne pathogens. In order to control pathogens in foodstuffs, efficient detection and inspection approaches are indispensable. Traditional microbiological approaches have been regarded as one standard practice for detecting and identifying pathogens in foodstuff for almost a century and even till now, they are dependable standard for guaranteeing food security. In general, these approaches only rest with the adoption of specific agar media to achieve the separation and calculation of viable bacterial cells in specimens. The steps of this kind of approach generally contain microbiological culturing and pathogens' segregation, and confirmation through biochemical and/or serological experiments, which needs five to seven days to achieve a totally reliable outcome for a certain pathogenic system [4]. However, though these traditional approaches are dependable, they are time consuming and labour-intensive as well, so as for guaranteeing modern food quality as well as instant response to potential risks, they are not suitable. Owing to this, in the last 25 years, a large number of rapid approaches have been figured out to save the testing time. Methods that have undergone studies or are being studied at present include miniaturized biochemistry experiments, physiochemical approaches which have bacterial metabolites measured, nucleic acid-based experiments that are very specific, antibody-based approaches, as well as completely automated instrumental diagnostic mechanisms [5]. The majority of these time-saving approaches developed previously have been reviewed by various groups broadly [6, 7]. Up to now, To date, well-researched quick approaches like enzyme linked immunosorbent assay (ELISA) as well as polymerase chain reaction (PCR) have cut down the testing time to 10–24 h and 4–6 h, respectively, and have realized limits of detection from  $10^1$  to  $10^6$  cfu/ml (cfu = colony forming units). In recent years, in order to detect pathogenic bacteria effectively, a variety of biosensors have been invented owing to their higher speed, sensitivity as well as dependability. As for a common biosensor, its sensitivity is within the range of  $10^3$  and  $10^4$  cfu/ml, whose testing time is approximately 2 hour under ideal environment [8-11].

On the other side, biosensors are applied as highly sensitive and specific instruments to realize the timely detection of the bacteria being emphasized. There are several effective biosensors of microbial inoculum that have been developed successfully [12-15]. A lot of fabricated impedimetric immunosensors have been put forward for detecting *S. aureus* ATCC 25923 within the range of 10-

$10^3$  CFU/mL [16-18]. Nevertheless, in the bacterial analysis of water or clinical specimens, the lower limit of detection is quite needed, because the infectious doses of *S. aureus* ATCC 2592 are generally fewer than ten cells. The results of research relevant to one-step synthesis of reduced graphene oxide (rGo)-Cu(II) nanocomposite that is economical as well as eco-friendly are presented in this essay. And then, aiming to detect water-borne pathogen (*S. aureus* ATCC 25923), this biosensing system has been employed. It shows that the binding power between the antibody and the substrate can be enhanced by the rGO-Cu(II) nanocomposite. Moreover, cysteine venner rock not only functions as versatile interface that can be functionalized easily through target molecules, but also it can sustain bioactivity of antibodies as well as strengthened water solubility of the material after synthesis.

## 2. EXPERIMENTS

### 2.1. Chemicals

Sigma is the material source of Graphite powder, *N,N*-dimethylacetamide (DMAC), copper(II) chloride dihydrate, L-Cysteine (Cys), Sodium azide ( $\text{NaN}_3$ ), *N*-ethyl-*N*-(3-dimethylaminopropyl) carbodimide (EDC), *N*-hydroxysuccinimide (NHS), as well as all other reagents and solvents of analysis level. The source of monoclonal antibodies as well as the target cells of *E. coli* (O157: H7) is Kirkegaard & Perry Laboratories and Gaithersburg MD, USA, respectively. Through the combination of phosphate buffer with 0.9% NaCl, the preparation of phosphate buffer saline (PBS) was finished. Mill-Q water was adopted in the whole experiments.

### 2.2. Synthesis of rGO-Cu(II) nanocomposite

As for synthesizing rGO-Cu(II) nanocomposite, firstly water solution of  $\text{CuCl}_2$  (1 M) was put into L-Cys solution in diverse concentration and the sonication of the solution took up 5 min. After this, in Cys-based Cu (II) with diverse concentrations, 0.1 mg/mL of GO dispersion was put in, and the sonication of the solution passed through 10 min until the colour turned into deep blue-grey from brown. The reference tests were conducted under the same conditions without Cu (II). After 6 hours' reaction at the temperature of 25 °C, the observation of the growth course of both the rGO-Cu(II) nanocomposite was realized.

### 2.3. Bacterial strains as well as conditions of growth

In this work, *S. aureus* ATCC 25923 was adopted. In the tests, cells developed at the temperature of 37 °C in tryptic soy broth (TSB, Difco) for one day. Natural seawater (100 mL) was obtained from the coast of Monastir (salinity 4 ‰, pH 8.0), and the water filtered through membranes (pore size, 0.22  $\mu\text{m}$ ; Millipore Corp., Bedford, MA), and underwent autoclaved treatment at 121 °C for 20 min. After this, *S. aureus* cells were rinsed thrice through centrifugation (13,000 rpm for 10 min)

with seawater after being autoclaved. The microcosms (100 mL) were added with these suspensions (about  $10^8$  CFU/mL) and then cultured in a stationary state at the indoor temperature.

#### 2.4. Immunosensor development

The rGO-Cu(II)/Au electrodes were processed with a combination of 2 mM EDC and 5 mM NHS for one hour at the temperature of 25 °C under dark environment to stimulate the —COOH groups revealed on the appearance of the electrode. And then, the incubation of the modified electrodes was accomplished through monoclonal antibodies ( $E_{cAb}$ , 20  $\mu$ l; 0.1 mg/mL) solution in a moist room for one night at indoor temperature (25 °C). With the use of PBS solution, the electrodes were rinsed in order to get rid of the extra unbound antibodies. Subsequently, antibodies-immobilized electrodes were processed with 1% bovine serum albumin (BSA) with the purpose of obstructing the non-specific binding sites followed by washing through PBS.

#### 2.5. Instrument

In order to study the development of rGO-Cu(II), Fourier transform infrared (FT-IR) spectroscopy measurements were conducted with the use of Perkin-Elmer spectrometer at room temperature. The implementation of electrochemical research was achieved through Autolab potentiostat/galvanostat with the adoption of one three-electrode cell, in which the working electrode was undertaken by Au, while the auxiliary electrode and reference electrode were undertaken by platinum and Ag/AgCl in phosphate buffer (PBS, 100 mM, pH 7.4, 0.9% NaCl) comprising 5 mM  $[\text{Fe}(\text{CN})_6]^{3-/4-}$  respectively.

### 3. RESULTS AND DISCUSSION

Outcomes of FTIR spectroscopy measurements of GO reveal dramatic peaks at 1624, 3413 as well as  $1396\text{ cm}^{-1}$  in accordance with C=O stretching vibration, O—H stretching and deformation, respectively (Figure 1A) [19, 20]. While at  $1247$  and  $1035\text{ cm}^{-1}$ , the summits in accordance with the existence of epoxy C—O stretching vibration as well as the alkoxy C—O stretching vibration can be seen clearly. The summits of the FTIR spectrum of rGO-Cu(II) are showed at  $2863\text{ cm}^{-1}$  and  $2924\text{ cm}^{-1}$  in conformity with stretching vibrations of alkane group (Figure 1B). The introduction of secondary amide groups was achieved through the appearance of Cys on the graphene sheets, which is similar to what revealed when the secondary amine peak occurred at approximately. A change of in the sites of  $\text{COO}^-$  and  $\text{NH}^{3+}$  is possible to be caused by a vibration in the dipole moment at the time that rGO-Cu(II) binds with the rGO surface with excellent electron density [21].

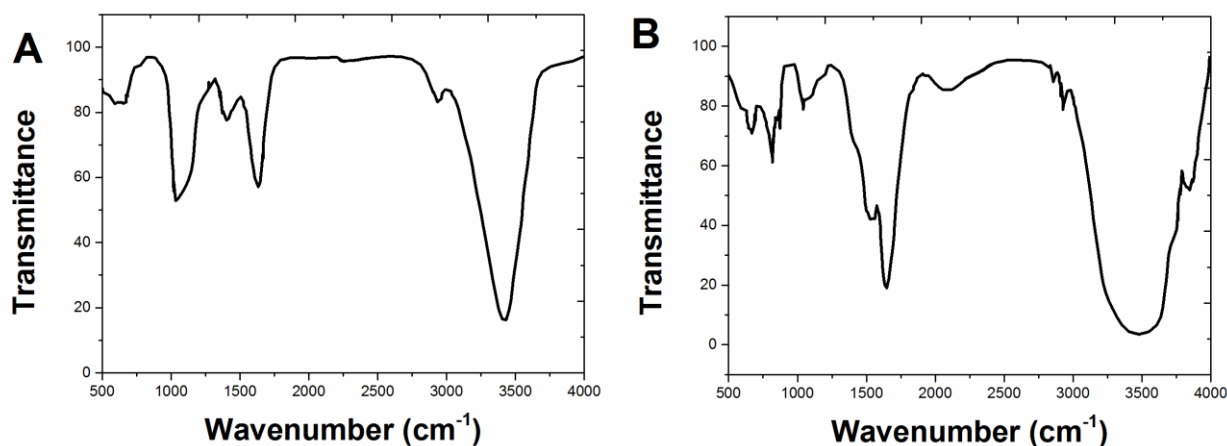


**Figure 1.** FTIR spectra of (A) GO as well as (B) rGO-Cu(II).

The UV-vis spectrum reveals the development of GO clearly in which the observation of a  $\pi$ - $\pi^*$  absorption band at 222 nm can be achieved (Figure 2A). However, the summit changed to 230 nm under the condition of rGO-Cu(II), as well as a shoulder  $n$ - $\pi^*$  absorption band at 305 nm could be seen. The absorption summit shows that several groups on the surface of the GO were likely to be removed, leading to the development of conjugated structure [22, 23]. Therefore, both the red shift phenomenon and disappearance of shoulder absorption peak indicated the successful reduction of GO to RGO.

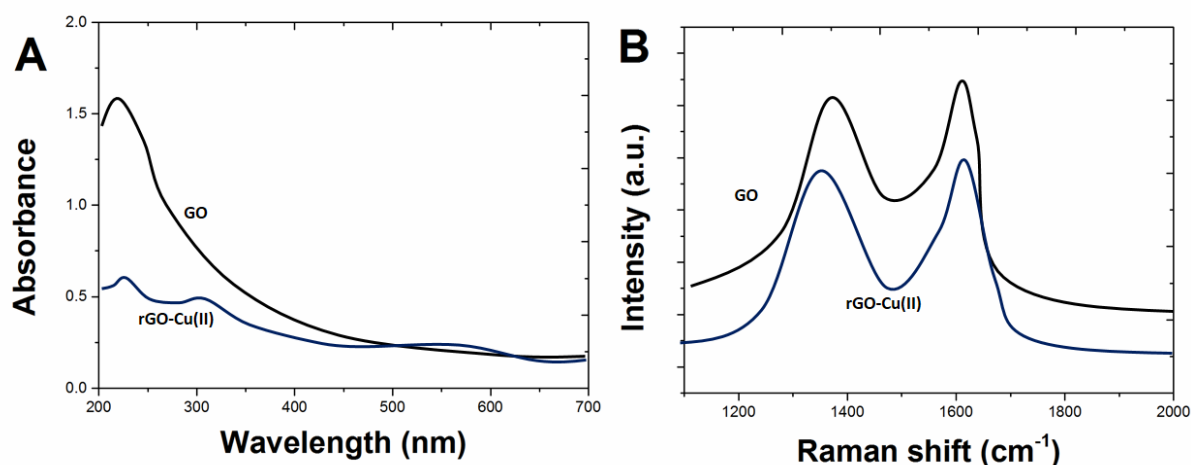


**Figure 2.** (A) UV-visible spectra and (B) Raman spectra of GO as well as rGO-Cu(II).

In order to research the Raman scattering in rGO-Cu(II) (Figure 2B), this work adopted Raman spectroscopic analysis. The G-band of GO is observed at  $\sim 1604 \text{ cm}^{-1}$  but an intense D-band summit occurs at  $\sim 1371 \text{ cm}^{-1}$  that corresponds to  $\text{sp}^3$  carbon as well as defects connected with vacancies and crystal boundaries (Figure 2B). Figure 2B demonstrated the results of the continuous decrease of GO and synthesis of rGO-Cu(II) nanocomposites. Owing to the excellent recovery capacity of the hexagonal system of carbon atom, the G band of rGO-Cu(II) nanocomposite was changed

to  $1611\text{ cm}^{-1}$ . In comparison with GO, rGO-Cu(II) possesses higher intensity ratio of D and G band ( $I_D/I_G$ ), indicating that the average size of the  $sp^2$  domains decreased and certain oxygen containing functional groups were removed as to RGO [24, 25].

The electrochemical impedance spectroscopy (EIS) is one of the most widely applied electrochemical tools, owing to its rapid and sensitive response happening at the interface of electrode-electrolyte [26]. In general, EIS contains a semicircle part which was seen at higher frequencies, in accordance with the electron transfer limited course, followed by a linear portion characterized by the lower frequencies caused by a diffusion limited electrode transport [27]. The value of charge transfer resistance ( $R_{ct}$ ) is offered by EIS spectra's semicircle diameter. The rise in the semicircle's diameter corresponds to an rise in the  $R_{ct}$ , and the quantitative value of  $R_{ct}$  can be obtained from testing impedance spectra through fitting one equivalent model on the basis of modified Randles as well as Ershler model to the data [28]. The shift in  $R_{ct}$  value when each modification procedure was finished was investigated with the adoption of phosphate buffer (PBS, 100 mM, pH 7.4, 0.9% NaCl) including 5 mM  $[\text{Fe}(\text{CN})_6]^{3-/4-}$  applied as the redox probe. Under the ideal state, the vacant Au electrode revealed nearly a straight line characterised by large scale diffusion limiting process where the  $R_{ct}$  value was  $30\ \Omega$  (Figure 3). When self-assembly of the Cys, CysCu, rGO-Cys, rGO-CysCu as well as on the Au electrode was accomplished,  $R_{ct}$  was observed to be 244.4, 185.7, 145.3, and  $122.1\ \Omega$  in order. The decline in the value of  $R_{ct}$  showed that adding Cu in the rGO-Cu(II) mechanism remarkably shifted the reactivity, resulting in more physical or chemical interaction between Cys and GO in comparison with that of original GO.

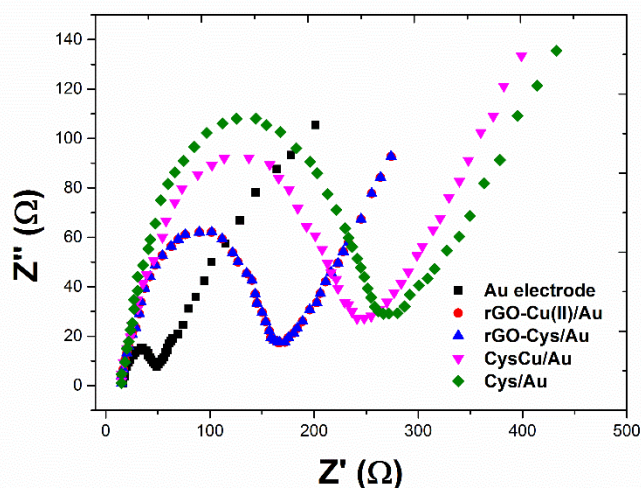


**Figure 3.** Electrochemical impedance spectra showing the change in  $R_{ct}$  value for the different modified Au electrode, rGO-Cu(II)/Au, rGO-Cys/Au, CysCu/Au and Cys/Au. (PBS, 100 mM, pH 7.4, 0.9% NaCl) containing 5 mM  $[\text{Fe}(\text{CN})_6]^{3-/4-}$ .

Nevertheless, the covalent binding of  $\text{Ec}_{\text{Ab}}$  together with the later withdrawal of the antibodies stucked in a physical way and obstruction of exposed carboxyl groups of the Au electrode after modification led to a rise of  $R_{ct}$  inside every case. This is likely to be caused by the binding of antibodies without conductivity, which obstructed the charge transfer course (Figure 4A and 4B). The antibody-antigen complex appeared at the time that the objective  $\text{Ec}_{\text{cells}}$  were incubated on the surface

of antibody modified electrode. The development of this complex led to increased barrier on account of cell membrane thickness (5–10 nm) as well as resistance ( $10^2$ – $10^5 \Omega \text{ cm}^2$ ) for the course of electrochemical transduction, thus blocking the redox probe's access to the surface of the electrode, leading to further rise in  $R_{ct}$ . The fitting values for a variety of equivalent circuit elements and the variation in the value of  $R_{ct}$  for these two electrodes are showed through the histogram. As a result, it can be signified that the solution resistance ( $R_s$ ) and Warburg resistance ( $Z_W$ ) remain unchanged, because the attributes of solution and diffusion of  $[\text{Fe}(\text{CN})_6]^{3-/4-}$  over the interface, respectively. In the impedance spectra, the electron-transfer kinetics completely takes charge of the electrode reaction. Cyclic voltammetry's summit current varies as a function of the square root of scan speed, indicating linear dependence of summit currents as for the scan speed. It can be seen that the electron transfer from rGO-Cys/Au as well as rGO-Cu(II)/Au electrodes is one surface-controlled course.

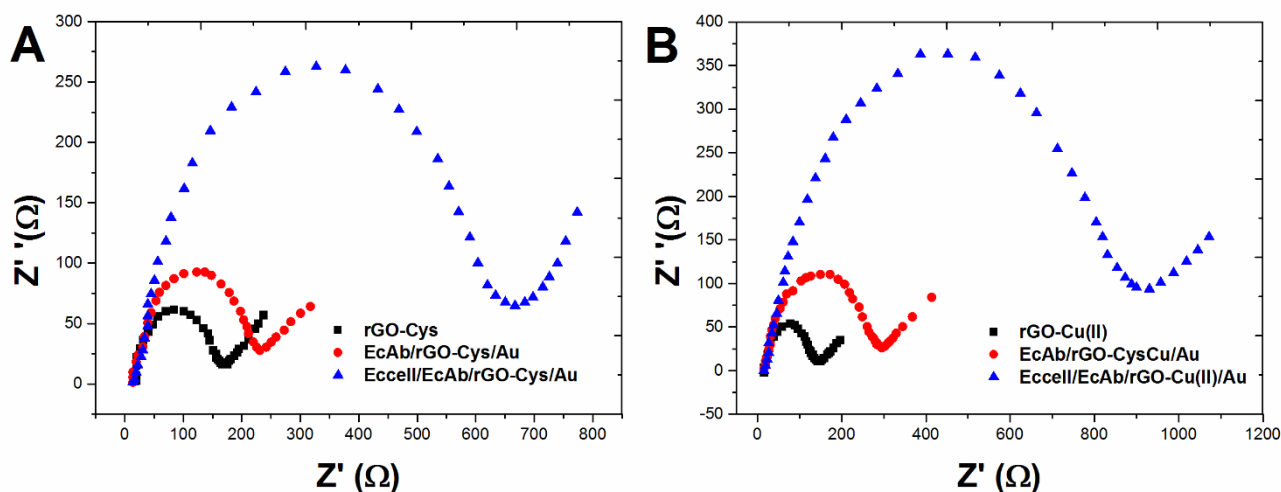


**Figure 4.** Nyquist diagram ( $Z_{im}$  versus  $Z_{re}$ ) for the Faradic impedance calculated in PBS (100 mM, pH 7.4, 0.9% NaCl) containing 5 mM  $[\text{Fe}(\text{CN})_6]^{3-/4-}$  within the frequency scope of  $10^6$  -  $10^{-2}$  Hz for electrodes of  $\text{Ec}_{Ab}/\text{rGO-Cys}/\text{Au}$ , (A) rGO-Cys,  $\text{Ec}_{cell}/\text{Ec}_{Ab}/\text{rGO-Cys}/\text{Au}$  as well as (B) rGO-Cu(II),  $\text{Ec}_{Ab}/\text{rGO-CysCu}/\text{Au}$ , and  $\text{Ec}_{cell}/\text{Ec}_{Ab}/\text{rGO-Cu(II)}/\text{Au}$ .

Non-Faradaic impedance biosensors perform impedance measurement in the absence of any redox probe. Bacteria detection is based on the impedance change upon the attachment of bacterial cells on an interdigitated microelectrode in the absence of any redox probe in the sample solution [29]. EIS was adopted to determine *S. aureus* cells quantitatively, because it offers a prompt response, indicating the electron transfer efficiency between the electro-active materials and the cover of the electrode. Through observation, we found there was a linear rise in impedance together with a rise in the dosage of *S. aureus* ATCC 25923 cells, showing that a resistant and capacitive dual layer between the electrolyte and the surface were formed. The response characterized by the  $\text{Ec}_{Ab}/\text{rGO-Cu(II)}/\text{Au}$  bioelectrode (Figure 5A) revealed that the number of cells that could be detected was more compared with that in  $\text{Ec}_{Ab}/\text{rGO-Cys}/\text{Au}$  bioelectrode ( $50$ – $10^8$  CFU/m ; Figure 5B) on account of the uplifted obstruction effect. These results have indicated that antibodies for specific recognition of target cells are not necessary immobilized directly on the sensor (e.g. electrode) surfaces [30].

The detection limit figured out with the use of the expression  $3\sigma/\text{sensitivity}$ , in which  $\sigma$  is representative of the standard deviation of the bare electrode, since the  $E_{cAb}/rGO-Cu(II)/Au$  bioelectrode (4.4 CFU/mL) is much less compared to that of  $E_{cAb}/rGO-Cys/Au$  bioelectrode (32 CFU/mL). Owing to the improved electron transfer speed from rGO-Cu(II) as well as highly specific immune reaction of antigen and antibody, the EIS detection performance was enhanced to a great extent. Under the condition of the rGO-Cys electrode, the antibodies were less accessible to developing antigen-antibody compound, leading to a decline in the sensitivity[31]. The linear relationship between bacterial concentration with  $\Delta R_{ct}$  was shown in Figure 6. The sensitivity of the proposed sensor was compared with that of other reported bacteria sensors and the results were presented in Table 1. Throughout the whole sensing experiments, the control signal was taken on by  $R_{ct}$  of anticorps-fixed on the electrode after modification with PBS solution.

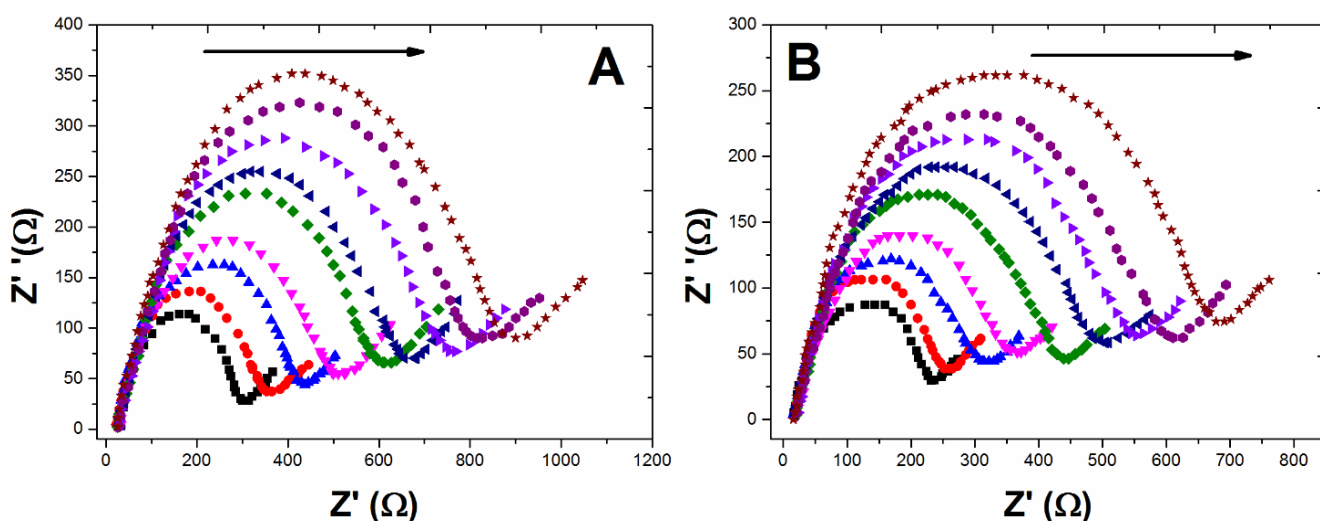


**Figure 5.** EIS revealing the immunosensing response for (A)  $E_{cAb}/rGO-Cu(II)/Au$  electrode as well as (B)  $E_{cAb}/rGO-Cys/Au$  electrode. (PBS, 100 mM, pH 7.4, 0.9% NaCl) containing 5 mM  $[Fe(CN)_6]^{3-/4-}$ .

**Table 1.** Comparison of the present sensor with other electrochemical bacteria sensors.

Electrode	Target bacteria	Detection limit	Reference
High density microelectrode	<i>E. coli</i> O157:H7.	$10^6$ CFU/mL	[29]
EIS	<i>E. coli</i> O157:H7.	1044 CFU/mL	[32]
Enzyme-labeled Amperometric Immunosensor	<i>L. monocytogenes</i>	$10^3$ CFU/mL	[33]
In-situ immuno-gold-ELISA	<i>S. typhimurium</i>	15 CFU/mL	[34]
$E_{cAb}/rGO-Cu(II)$	<i>Staphylococcus aureus</i>	4.4 CFU/mL	This work

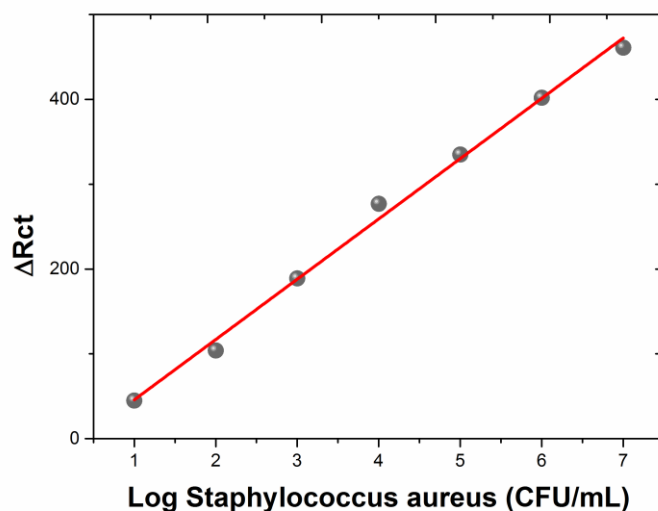


**Figure 6.** The linearity plot with variation in the concentration of *Staphylococcus aureus* cells

In order to evaluate reproducibility as well as dependability of the immunosensor presented, the coefficient of variation ( $C_oV$ ) of inter-testing precision was adopted with dual specimens including  $1 \times 10^1$  CFU/mL as well as  $1 \times 10^3$  CFU/mL of  $E_{c_{cells}}$ . The testing time  $C_oV$  was assessed through analyzing the equal concentration of  $E_{c_{cells}}$  ( $10^1$  CFU/mL and  $10^3$  CFU/mL) with the use of five same electrodes. Five immunosensors which were prepared independently showed similar current response and the inter-testing  $C_oV$  was made sure to be 5.2% ( $10^1$  CFU/mL) and 3.4% ( $10^3$  CFU/mL). The low value of relative standard deviation showed that the immunosensor put forward showed excellent repeatability. Besides, the immunosensor's storage stability was evaluated through putting the  $E_{c_{Ab/rGO-Cu(II)/Au}}$  electrode in an icebox and calculating its response towards *S. aureus* ATCC 25923 detection every five days. When one month passed over, the impedimetric response of the sensor was still 93.5% of the previous value showing that the immunosensor with good reliability and enhanced stability could be adopted for the biocompatibility of the Cys that retained the antibodies as well other biomolecules.

#### 4. CONCLUSIONS

In this paper, an immunosensor with high sensitivity was formed for the recognition of the emphasized and resuscitated pathogenic *S. aureus* bacteria. The special immobilized antibodies as well as bacteria interaction impedance spectroscopy were mostly characterized by the impedance spectroscopy. With the use of *S. aureus* antibody, a wider detection scope ( $10-10^8$  CFU/mL) as well as a much smaller detection limit (4.4CFU/mL) with great specificity of  $E_{c_{Ab/rGO-Cu(II)/Au}}$  electrode towards *S. aureus* detection has been realized successfully.

#### References

1. S. Altekruze and D. Swerdlow, *The American journal of the medical sciences*, 311 (1996) 23.
2. P. Mead, L. Slutsker, V. Dietz, L. McCaig, J. Bresee, C. Shapiro, P. Griffin and R. Tauxe, *Emerging*

- Infectious Diseases*, 5 (1999) 607.
3. R. STIER, *Journal of Rapid Methods & Automation in Microbiology*, 2 (1993) 17.
  4. B. Swaminathan and P. Feng, *Annual Reviews in Microbiology*, 48 (1994) 401.
  5. L. Yang and R. Bashir, *Biotechnology Advances*, 26 (2008) 135.
  6. H. Van Der Zee, *Journal of AOAC International*, 80 (1996) 934.
  7. D. Ivnitski, I. Abdel-Hamid, P. Atanasov and E. Wilkins, *Biosensors and Bioelectronics*, 14 (1999) 599.
  8. M. Abdalhai, A.n.M. Fernandes, X. Xia, A. Musa, J. Ji and X. Sun, *Journal of agricultural and food chemistry*, 63 (2015) 5017.
  9. R. Miranda-Castro, M. Lobo-Castañón, A. Miranda-Ordieres and P. Tuñón-Blanco, *Electroanalysis*, 22 (2010) 1297.
  10. J. Lee, A. Tatsumi, K. Abe, W. Yoshida, K. Sode and K. Ikebukuro, *Analytical Methods*, 6 (2014) 4991.
  11. X. Wang, P. Zhu, F. Pi, H. Jiang, J. Shao, Y. Zhang and X. Sun, *Biosensors and Bioelectronics*, 81 (2016) 349.
  12. M. Mejri, A. Tlili and A. Abdelghani, *International Journal of Electrochemistry*, 2011 (2011)
  13. M. Mejri, H. Baccar, E. Baldrich, F. Del Campo, S. Helali, T. Ktari, A. Simonian, M. Aouni and A. Abdelghani, *Biosensors and Bioelectronics*, 26 (2010) 1261.
  14. M. Varshney and Y. Li, *Biosensors and Bioelectronics*, 24 (2009) 2951.
  15. B. Byrne, E. Stack, N. Gilmartin and R. O'Kennedy, *Sensors*, 9 (2009) 4407.
  16. J. Liu, K. Settu, J. Tsai and C. Chen, *Electrochimica Acta*, 182 (2015) 89.
  17. N. Baram, D. Starosvetsky, J. Starosvetsky, M. Epshtein, R. Armon and Y. Ein-Eli, *Electrochimica Acta*, 54 (2009) 3381.
  18. W. Dou, W. Tang and G. Zhao, *Electrochimica Acta*, 97 (2013) 79.
  19. Y. Zhao, X. Song, Q. Song and Z. Yin, *Crystengcomm*, 14 (2012) 6710.
  20. M. Schriver, W. Regan, W. Gannett, A. Zaniwski, M. Crommie and A. Zettl, *Acs Nano*, 7 (2013) 5763.
  21. C. Pandey, I. Tiwari, V. Singh, K. Sood, G. Sumana and B. Malhotra, *Sensors & Actuators B Chemical*, 238 (2016) 1060.
  22. B. Jiang, Y. Liang, Q. Wu, H. Jiang, K. Yang, L. Zhang, Z. Liang, X. Peng and Y. Zhang, *Nanoscale*, 6 (2014) 5616.
  23. K. Kudin, B. Ozbas, H. Schniepp, R. Prud'Homme, I. Aksay and R. Car, *Nano Letters*, 8 (2008) 36.
  24. X. Li, Q. Wang, Y. Zhao, W. Wu, J. Chen and H. Meng, *Journal of Colloid and Interface Science*, 411 (2013) 69.
  25. S. Kamada, H. Nomoto, K. Fukuda, T. Fukawa, H. Shirai and M. Kimura, *Colloid Polym Sci*, 289 (2011) 925.
  26. C. Pandey, A. Sharma, G. Sumana, I. Tiwari and B. Malhotra, *Nanoscale*, 5 (2013) 3800.
  27. A. Ramanavicius, A. Finkelsteinas, H. Cesiulis and A. Ramanaviciene, *Bioelectrochemistry*, 79 (2010) 11.
  28. J. Randles, *Discussions of the Faraday Society*, 1 (1947) 11.
  29. S.M. Radke and E.C. Alcocilja, *Biosensors & bioelectronics*, 20 (2005) 1662.
  30. L. Yang and R. Bashir, *Biotechnology Advances*, 26 (2008) 135.
  31. M. He and A.E. Herr, *Nature Protocol*, 5 (2010) 1844.
  32. C. Ruan, L. Yang and Y. Li, *Anal. Chem.*, 74 (2002) 4814.
  33. Y. Zheng and A. Rundell, *IEEE Transactions on Nanobioscience*, 2 (2003) 14.
  34. I. Cho and J. Irudayaraj, *International Journal of Food Microbiology*, 164 (2013) 70.